arXiv:2405.09956v1 [cond-mat.mtrl-sci] 16 May 2024

Data-Assimilated Crystal Growth Simulation for Multiple Crystalline Phases

Yuuki Kubo,[1, *] Ryuhei Sato,[2] Yuansheng Zhao,[3] Takahiro Ishikawa,[1] and Shinji Tsuneyuki[1]
[1] *Department of Physics, The University of Tokyo,*
7-3-1 Hongo, Bunkyo-ku, Tokyo 113-0033, Japan
[2] *Department of Materials Engineering, The University of Tokyo,*
7-3-1 Hongo, Bunkyo-ku, Tokyo 113-8656, Japan
[3] *Institute of Materials and Systems for Sustainability, Nagoya University,*
Furo-cho, Chikusa-ku, Nagoya, Aichi 464-8601, Japan

(Dated: May 17, 2024)

To determine crystal structures from an X-ray diffraction (XRD) pattern containing multiple unknown phases, a data-assimilated crystal growth (DACG) simulation method has been developed. The XRD penalty function selectively stabilizes the structures in the experimental data, promoting their grain growth during simulated annealing. Since the XRD pattern is calculated as the Fourier transform of the pair distribution function, the DACG simulation can be performed without prior determination of the lattice parameters. We applied it to C (graphite and diamond) and SiO_2 (low-quartz and low-cristobalite) systems, demonstrating that the DACG simulation successfully reproduced multiple crystal structures.

Crystal structure determination is an essential process in materials science to predict and understand the properties of materials. Experimental researchers mainly rely on X-ray diffraction (XRD) measurements or neutron diffraction (ND) spectroscopy to determine crystal structures. To analyze new structures from powder XRD data, we first determine their lattice parameters. Recent developments in crystallographic methodology have made it possible to systematically determine lattice parameters from single-phase XRD patterns [1–6]. On the other hand, because the peak assignment of XRD data significantly increases the number of wrong lattice parameter candidates, it is still challenging to find the correct lattice parameters from XRD data reflecting multiple unknown phases.

Computational science has also contributed to crystal structure determination, especially when it is difficult to determine the structure through experimental techniques [7]. In computational science, crystal structure has been predicted by finding the global minimum of the physical interatomic potential energy. To overcome the potential energy barrier between local minima and the global minimum, metaheuristics methods based on random sampling [8], particle-swarm optimization [9, 10], genetic algorithms [11–13], *etc.*, have been employed with first-principles calculations in recent years. Indeed, these methods successfully determined the new structures such as high-temperature superconducting hydrides under ultra-high pressure [14–22]. In addition, combined with machine learning potentials, they can correspond to the variable composition analysis [23–25]. Nevertheless, since these methods still require high computational costs, there is also a demand for computational approaches directly referring to the experimental data.

Under such circumstances, one possible way to accomplish rapid and accurate optimization is to supplement theoretical simulations with experimental data [26–30], and we have developed an experimental data-assimilated molecular dynamics (DAMD) simulation using XRD and ND data. Our previous study confirmed that the DAMD simulation can efficiently determine the target crystalline [31, 32] and amorphous [33] structures. However, these simulations require the lattice parameters to be determined in advance [32] and do not work well when XRD data contain peaks from multiple unknown crystalline phases. In this study, we propose a data-assimilated crystal growth (DACG) simulation method, which is applicable to the structure determination even in those cases.

Figure 1 shows a schematic image of the DACG simulation proposed in this study. Here, we assume that the experimental XRD data contain peaks from multiple unknown phases, and the lattice parameters cannot be readily determined. Therefore, in the DACG simulation, we employ large simulation cells including a few thousand atoms to obtain grains of the target crystal structures rather than the perfect crystals.

To obtain crystal grains, MD simulations of crystal growth are performed and accelerated by employing the cost function F [31–33]:

$$F(\mathbf{R}) = E(\mathbf{R}) + \alpha N D[I_{\mathrm{ref}}(Q), I_{\mathrm{calc}}(Q;\mathbf{R})], \qquad (1)$$

where $\mathbf{R}$ is the atomic coordinates and E is the interatomic potential energy. I_{ref} and I_{calc} are the XRD intensity referred from experimental data and that calculated from a structure in the simulation, respectively. D is the XRD penalty function that represents the dissimilarity between I_{ref} and I_{calc}. α is the weight parameter, N is the number of atoms, and Q is the magnitude of the scattering vector. Most of the structures inconsistent with the experimental data are destabilized by the cost function F as shown in Fig. 1. Therefore, DA can increase the probability of reaching the target structures through optimization.

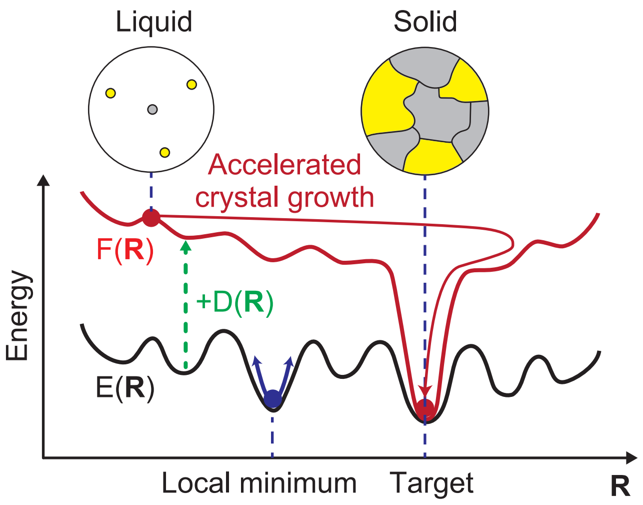

FIG. 1. Schematic image of the data-assimilated crystal growth (DACG) simulation. The DACG simulation employs a simulation cell that is sufficiently large compared to the unit cells of the crystal structures. Crystal growth simulations are accelerated by changing the potential energy surface from the interatomic potential $E(\mathbf{R})$ to the cost function $F(\mathbf{R})$, where $\mathbf{R}$ represents the atomic coordinates. Note that the cost function $F(\mathbf{R})$ is the linear sum of the interatomic potential $E(\mathbf{R})$ and the XRD penalty function $D(\mathbf{R})$.

Following our previous study [32], we used a penalty function D based on the correlation coefficient:

$$D = 1 - \frac{\int \mathrm{d}Q\,(I_{\mathrm{ref}} - \overline{I}_{\mathrm{ref}})(I_{\mathrm{calc}} - \overline{I}_{\mathrm{calc}})}{\sqrt{\int \mathrm{d}Q\,(I_{\mathrm{ref}} - \overline{I}_{\mathrm{ref}})^2}\sqrt{\int \mathrm{d}Q\,(I_{\mathrm{calc}} - \overline{I}_{\mathrm{calc}})^2}}, \tag{2}$$

where $\overline{I}$ is the averaged XRD intensity over the integral range of Q. By defining D in this way, we can simultaneously compare the peak positions and intensities of I_{ref} and I_{calc}.

In addition, we adopted the following formula to calculate I_{calc}:

$$\frac{I_{\mathrm{calc}}}{L(2\theta)} \propto \sum_{\mu} c_\mu f_\mu^2(Q) + \sum_{\mu,\nu} c_\mu c_\nu f_\mu(Q) f_\nu(Q) \times \int_0^{r_{\mathrm{cutoff}}} \mathrm{d}r\, 4\pi r^2 \rho_0 [g_{\mu\nu}(r) - 1] \frac{\sin Qr}{Qr}, \tag{3}$$

where 2θ is the angle between the incident and scattered X-rays, $L(2\theta)$ is the polarization factor, c_μ is the ratio of atomic species μ, $f_\mu(Q)$ is the atomic form factor, ρ_0 is the number of atoms per volume, and $g_{\mu\nu}(r)$ is the partial pair distribution function (PDF) between atomic species μ and ν. r_{cutoff} is the cutoff radius for calculating PDF. Since Eq. (3) does not include any lattice parameters and Laue indices directly, we can perform the DACG simulation without any prior determination of the lattice parameters. Furthermore, this method reduces the computational cost by making the cutoff distance r_{cutoff} smaller. On the other hand, the drawback of this method is that the resolution of the calculated XRD peak position becomes inversely proportional to r_{cutoff}.

When the DACG simulations are performed using multi-phase XRD data as the reference, a polycrystalline structure containing multiple different crystal structures may be obtained in a single simulation cell. To extract the grains of each phase in those cases, we perform K-means clustering [34] based on the site-specific radial distribution function (SSRDF) around each atom i defined as

$$g_i(r) = \frac{1}{4\pi r^2 \rho_0} \sum_{j \neq i} \delta(r - r_{ij}) f_{\mathrm{cut}}(r), \tag{4}$$

where ρ_0 is the number of atoms per volume, and r_{ij} is the distance between atoms i and j. Here, $f_{\mathrm{cut}}(r)$ is a smooth cutoff function defined as

$$f_{\mathrm{cut}}(r) = \begin{cases} \frac{1}{2}\left[\cos\left(\pi \frac{r}{R}\right) + 1\right] & (r < R), \\ 0 & (r \geq R), \end{cases} \tag{5}$$

using cutoff radius R.

To test the effectiveness of the DACG simulation, we applied it to the structure determination of C (graphite and diamond) and $\mathrm{SiO_2}$ (low-quartz and low-cristobalite) polymorphs. We used the Large-scale Atomic/Molecular Massively Parallel Simulator (LAMMPS) [35, 36] package and the external code for calculating the penalty function implemented in our previous study [33]. The long-range carbon bond order potential (LCBOP) [37] for C and the Tsuneyuki potential [38] for $\mathrm{SiO_2}$ have been employed for the physical interatomic potential energy. The temperature was controlled by the velocity scaling method [39], and the time step was set to 0.5 and 1 fs for C and $\mathrm{SiO_2}$ simulations, respectively. XRD patterns from 0 to 4 $\mathrm{\AA}^{-1}$ were used to calculate the penalty function D. For calculating I_{calc} from structures during the DACG simulation, we set r_{cutoff} to 15 and 21-25 Å for C and $\mathrm{SiO_2}$ cases, respectively. As initial atomic configurations, 6000 and 10 200 atoms were randomly placed in cubic boxes for C and $\mathrm{SiO_2}$ cases, respectively. Here, the simulation cell size was determined so that the atomic density was consistent with the density of each desired crystal structure [40–42]. We performed simulated annealing with the cost function F (DA, data assimilation) and that with the interatomic potential E (SA, normal simulated annealing). First, since the initial configurations were energetically too unstable, we performed short MD simulations with small time steps without the XRD penalty function to relax the structure. Next, the temperatures were set at 14 000 and 10 000 K for C and $\mathrm{SiO_2}$, respectively, and then decreased linearly to 0 K in 0.5 and 5 ns. The weight parameter α of the XRD penalty function in Eq. (1) was set to 10 eV for both C and $\mathrm{SiO_2}$ cases in this study.

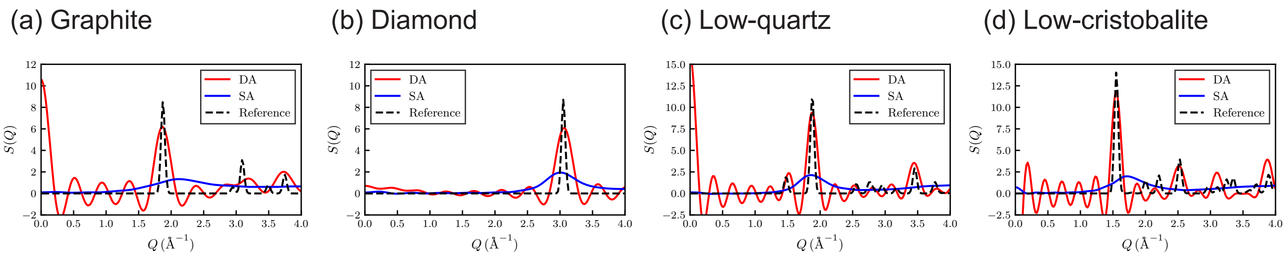

(a) Graphite (b) Diamond (c) Low-quartz (d) Low-cristobalite

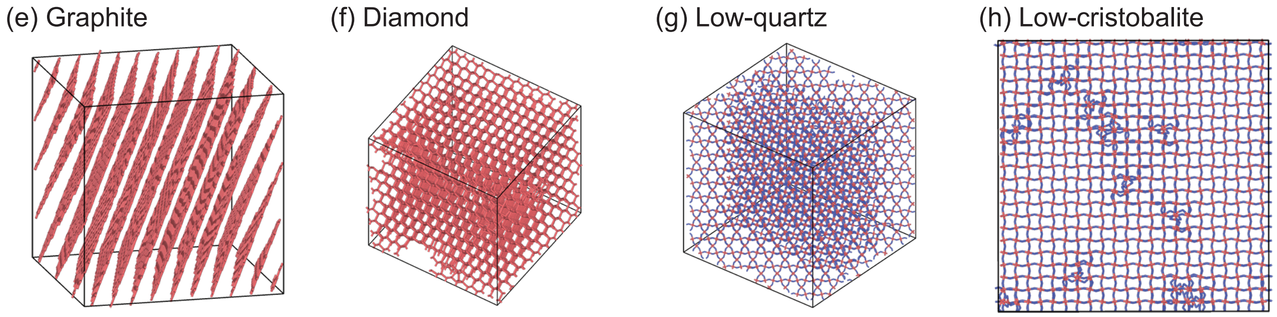

(e) Graphite (f) Diamond (g) Low-quartz (h) Low-cristobalite

FIG. 2. (Top) (a)-(d) Structure factors $S(Q)$ corresponding to the ideal structures (black dashed lines), and those of the structures obtained by normal simulated annealing (SA, blue solid lines) and data-assimilated simulations (DA, red solid lines) as functions of wavenumber Q. (Bottom) Snapshots of the structures obtained after the DACG simulations using single-phase XRD patterns of the ideal (e) graphite, (f) diamond, (g) low-quartz, and (h) low-cristobalite structures. These snapshots were drawn by OVITO [43].

First, we performed simulated annealing with the cost function F (Eq. (1)) using single-phase XRD data of graphite (C), diamond (C), low-quartz (SiO_2) and low-cristobalite (SiO_2). Figures 2(a)-(d) show the structure factors $S(Q)$, corresponding to the reference XRD pattern used for the DACG simulations (black dashed lines), and those calculated from the structures obtained by DA (red lines) and SA (blue lines). As shown in Figs. 2(a)-(d), no Bragg peaks appear in $S(Q)$ for the structures obtained by SA, suggesting that no ordered structures were obtained. On the other hand, peak positions of $S(Q)$ obtained by DA are comparable with those in the reference $S(Q)$. This suggests that the target structures were successfully obtained by DA owing to the XRD penalty function D. Figures 2(e)-(h) show the snapshots of the structures obtained after the DACG simulations. As shown in the snapshots, we successfully obtained the target structures: a layered structure like graphite in Fig. 2(e), a three-dimensional network originated from sp^3 hybrid orbitals formed over the whole simulation cell in Fig. 2(f), a triple-helical structure with some disordered parts in Fig. 2(g), and a network consisting only of six-membered rings in Fig. 2(h). These results suggest that the DACG simulations can determine the target structures correctly from single-phase XRD patterns without prior determination of the lattice parameters. Note that the small oscillations appearing in $S(Q)$ in the DA cases are caused by the Fourier transformation of PDF with the finite cutoff distance r_{cutoff} in Eq. (3).

Next, we conducted DACG simulations to determine multiple crystal structures from multi-phase reference XRD data. We used 1:1 mixture of the XRD patterns of ideal graphite and diamond structures as the reference XRD data (black dashed line) as shown in Fig. 3(a). The atomic density was set to the average of those of graphite and diamond. Figure 3(a) also shows the structure factors $S(Q)$ of the structures obtained by DA and SA. As shown in Fig. 3(a), peak positions of $S(Q)$ obtained after the DACG simulation (red solid line) agrees well with those of the ideal graphite and diamond peaks in the reference $S(Q)$, suggesting that the structure obtained by DA contains ordered structures related to the target ones. On the other hand, any peaks in the reference $S(Q)$ were not reproduced by SA, suggesting that SA without the penalty function D did not even yield any ordered structures. We can also see that the structure obtained by the DACG simulation indeed has some ordered structures shown in Fig. 3(c). However, it is difficult to conclude from only the snapshot whether this structure contains both graphite and diamond structures simultaneously. Therefore, we conducted K-means clustering to extract crystal grains from the obtained structure. Here, the number of groups for clustering was set to two so that the atoms could be classified into graphite and diamond phases, and the cutoff distance for the SS-RDF calculation was set to 5 Å. As the result of the clustering, the atoms were classified into two phases as shown in Figs. 3(d) and (e) which form graphite-like and

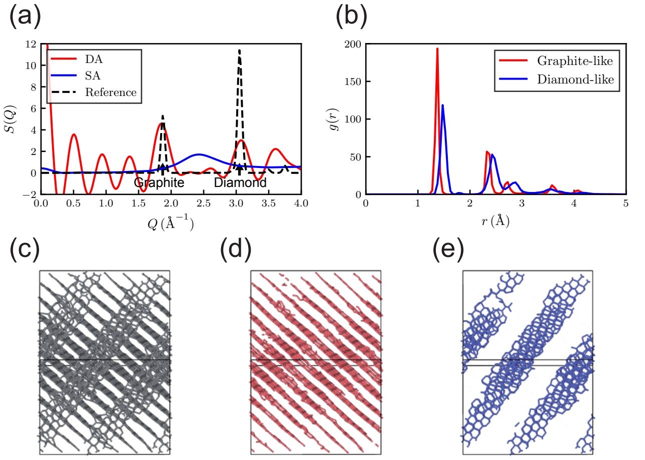

FIG. 3. (a) Structure factor $S(Q)$ corresponding to the reference XRD data (black dashed line), the structure obtained by normal simulated annealing (SA, blue solid line), and the structure obtained by the DACG simulation (DA, red solid line). (b) SSRDF averaged over center atoms in each phase. (c) A snapshot of the structure obtained after the DACG simulation using XRD data containing peaks of both graphite and diamond as the reference. (d) and (e) Atoms in the clusters obtained by K-means clustering.

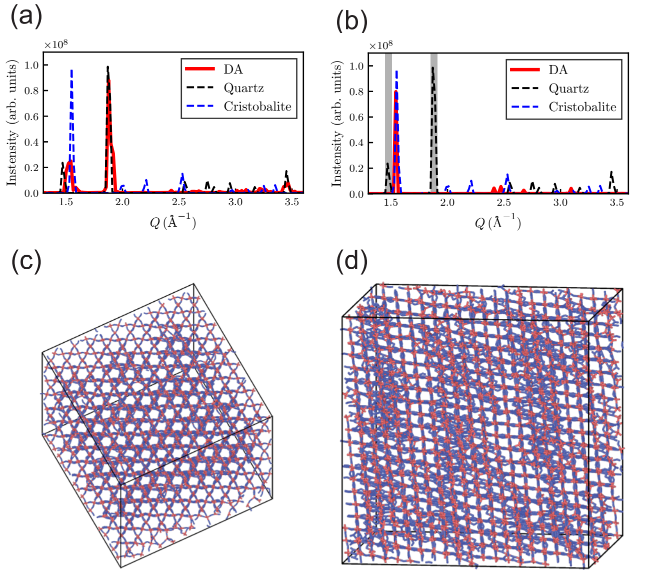

FIG. 4. (a) XRD patterns of low-quartz (black dashed line), low-cristobalite (blue dashed line), and the structure obtained after the first DACG simulation (red solid line). (b) Reference XRD pattern and the one of the structure obtained after the second DACG simulation, where XRD patterns in the range of $1.45 \leq Q \leq 1.5$ and $1.85 \leq Q \leq 1.9$ (masked area) were not used during the simulation. Note that all XRD patterns in these figures were calculated by using the lattice parameters of the simulation cell and Laue indices to analyze the obtained structure in detail. (c) A snapshot of the structure obtained by the first DACG simulation, using XRD data containing peaks of both low-quartz and low-cristobalite as the reference. (d) A snapshot of the structure obtained after the second DACG simulation.

diamond-like structures, respectively. Furthermore, the SSRDFs averaged over the center atoms in Figs. 3(d) (red line) and (e) (blue line) are shown in Fig. 3(b). As shown in this figure, it is confirmed that there are groups of atoms with different distances to the first and second nearest neighboring atoms and that the clustering successfully distinguished them. Thus, we concluded that, in the case of multi-phase C, graphite and diamond were obtained simultaneously by a single DACG simulation, and the grain of each phase was successfully extracted by K-means clustering using the SSRDF as an atomic fingerprint.

In the case of multi-phase SiO_2, all the target structures (low-quartz and low-cristobalite) were successfully reproduced by repeating the DACG simulation multiple times. Figure 4(a) shows the XRD patterns of ideal low-quartz and low-cristobalite, which were mixed in a 2.5:1 ratio and used as the reference XRD data in the DACG simulations. The mixing ratio of the XRD patterns was determined so that the maximum intensity of low-quartz and low-cristobalite XRD patterns take the same value. The atomic density was set to the average of those of low-quartz and low-cristobalite. Figure 4(a) also shows the XRD pattern calculated from the structure obtained after the first DACG simulation. This XRD pattern was calculated using the lattice parameters of the simulation cell and Laue indices to analyze the obtained structure in detail. Note that during the DACG simulation, XRD patterns were still calculated using Eq. (3). As shown in the figure, the first and second peaks of quartz were reproduced by the first DACG simulation. On the other hand, none of the peaks of cristobalite were reproduced by the first DACG simulation. This suggests that the first DACG simulation yielded only quartz-like ordered structures. Figure 4(c) shows the snapshot of the structure obtained by the first DACG simulation, in which a quartz-like triple-helical structure exists.

To obtain the crystal structures of the remaining phases, we conducted the DACG simulation again using the reference XRD data. However, this time, the powder XRD pattern in the range highlighted in gray in Fig. 4(b) was not used for calculating the XRD penalty function D during the simulation, since the structure corresponding to the peaks in those ranges has been already obtained by the previous DACG simulation. Figure 4(b) shows the XRD pattern calculated using the lattice parameters of the simulation cell and Laue indices from the structure obtained after the second DACG simulation. As shown in this figure, unlike the first DACG simulation, the second one reproduced the first peak of cristobalite. Furthermore, Fig. 4(d) shows a snapshot of the structure obtained by the second DACG simulation, in which a cristobalite-like structure can be seen. Thus, we conclude that in the case of multi-phase SiO_2, all the target structures were successfully obtained by the sequential DACG simulations, in which the XRD peaks related to the structures obtained at each DACG simulation are masked one by one.

In summary, we proposed a computer simulation method for efficiently growing and finding crystal structures by assimilating powder diffraction data from unknown crystalline phases. This method will help determine the crystal structures of new materials in combinatorial synthesis or under extreme conditions.

This work was supported by JSPS KAKENHI Grant numbers JP18H05519, JP24K00544, and JP20H05644. The computation in this work was partly performed by using the facilities of the Supercomputer Center, the Institute for Solid State Physics, The University of Tokyo. Y.K. is supported by MEXT - Quantum Leap Flagship Program (MEXT Q-LEAP).

---

* yuki.kubo@phys.s.u-tokyo.ac.jp

[1] J. W. Visser, Journal of Applied Crystallography **2**, 89 (1969).
[2] P.-E. Werner, L. Eriksson, and M. Westdahl, Journal of Applied Crystallography **18**, 367 (1985).
[3] A. Altomare, G. Campi, C. Cuocci, L. Eriksson, C. Giacovazzo, A. Moliterni, R. Rizzi, and P.-E. Werner, Journal of Applied Crystallography **42**, 768 (2009).
[4] A. Boultif and D. Louër, Journal of Applied Crystallography **37**, 724 (2004).
[5] A. Le Bail, Powder Diffraction **19**, 249–254 (2004).
[6] R. Oishi-Tomiyasu, Journal of Applied Crystallography **47**, 593 (2014).
[7] S. M. Woodley and R. Catlow, Nature Materials **7**, 937 (2008).
[8] C. J. Pickard and R. J. Needs, Journal of Physics: Condensed Matter **23**, 053201 (2011).
[9] Y. Wang, J. Lv, L. Zhu, and Y. Ma, Phys. Rev. B **82**, 094116 (2010).
[10] Y. Wang, J. Lv, L. Zhu, and Y. Ma, Computer Physics Communications **183**, 2063 (2012).
[11] A. R. Oganov and C. W. Glass, The Journal of Chemical Physics **124**, 244704 (2006).
[12] C. W. Glass, A. R. Oganov, and N. Hansen, Computer Physics Communications **175**, 713 (2006).
[13] T. Ishikawa and T. Miyake, Phys. Rev. B **101**, 214106 (2020).
[14] Y. Li, J. Hao, H. Liu, Y. Li, and Y. Ma, The Journal of Chemical Physics **140**, 174712 (2014).
[15] D. Duan, Y. Liu, F. Tian, D. Li, X. Huang, Z. Zhao, H. Yu, B. Liu, W. Tian, and T. Cui, Scientific Reports **4**, 6968 (2014).
[16] A. P. Drozdov, M. I. Eremets, I. A. Troyan, V. Ksenofontov, and S. I. Shylin, Nature **525**, 73 (2015).
[17] M. Einaga, M. Sakata, T. Ishikawa, K. Shimizu, M. I. Eremets, A. P. Drozdov, I. A. Troyan, N. Hirao, and Y. Ohishi, Nature Physics **12**, 835 (2016).
[18] F. Peng, Y. Sun, C. J. Pickard, R. J. Needs, Q. Wu, and Y. Ma, Phys. Rev. Lett. **119**, 107001 (2017).
[19] H. Liu, I. I. Naumov, R. Hoffmann, N. W. Ashcroft, and R. J. Hemley, Proceedings of the National Academy of Sciences **114**, 6990 (2017).
[20] Z. M. Geballe, H. Liu, A. K. Mishra, M. Ahart, M. Somayazulu, Y. Meng, M. Baldini, and R. J. Hemley, Angewandte Chemie International Edition **57**, 688 (2018).
[21] M. Somayazulu, M. Ahart, A. K. Mishra, Z. M. Geballe, M. Baldini, Y. Meng, V. V. Struzhkin, and R. J. Hemley, Phys. Rev. Lett. **122**, 027001 (2019).
[22] A. P. Drozdov, P. P. Kong, V. S. Minkov, S. P. Besedin, M. A. Kuzovnikov, S. Mozaffari, L. Balicas, F. F. Balakirev, D. E. Graf, V. B. Prakapenka, E. Greenberg, D. A. Knyazev, M. Tkacz, and M. I. Eremets, Nature **569**, 528 (2019).
[23] E. V. Podryabinkin, E. V. Tikhonov, A. V. Shapeev, and A. R. Oganov, Phys. Rev. B **99**, 064114 (2019).
[24] C. J. Pickard, Phys. Rev. B **106**, 014102 (2022).
[25] T. Ishikawa, Y. Tanaka, and S. Tsuneyuki, Phys. Rev. B **109**, 094106 (2024).
[26] M. W. Deem and J. M. Newsam, Journal of the American Chemical Society **114**, 7189 (1992).
[27] M. Falcioni and M. W. Deem, The Journal of Chemical Physics **110**, 1754 (1999).
[28] H. Putz, J. C. Schön, and M. Jansen, Journal of Applied Crystallography **32**, 864 (1999).
[29] O. J. Lanning, S. Habershon, K. D. Harris, R. L. Johnston, B. M. Kariuki, E. Tedesco, and G. W. Turner, Chemical Physics Letters **317**, 296 (2000).
[30] A. A. Coelho, Journal of Applied Crystallography **33**, 899 (2000).
[31] N. Tsujimoto, D. Adachi, R. Akashi, S. Todo, and S. Tsuneyuki, Phys. Rev. Mater. **2**, 053801 (2018).
[32] S. Yoshikawa, R. Sato, R. Akashi, S. Todo, and S. Tsuneyuki, The Journal of Chemical Physics **157**, 224112 (2022).
[33] Y. Zhao, R. Sato, and S. Tsuneyuki, Journal of Non-Crystalline Solids **600**, 122028 (2023).
[34] F. Pedregosa, G. Varoquaux, A. Gramfort, V. Michel, B. Thirion, O. Grisel, M. Blondel, P. Prettenhofer, R. Weiss, V. Dubourg, J. Vanderplas, A. Passos, D. Cournapeau, M. Brucher, M. Perrot, and E. Duchesnay, Journal of Machine Learning Research **12**, 2825 (2011).
[35] S. Plimpton, Journal of Computational Physics **117**, 1 (1995).
[36] A. P. Thompson, H. M. Aktulga, R. Berger, D. S. Bolintineanu, W. M. Brown, P. S. Crozier, P. J. in 't Veld, A. Kohlmeyer, S. G. Moore, T. D. Nguyen, R. Shan, M. J. Stevens, J. Tranchida, C. Trott, and S. J. Plimpton, Computer Physics Communications **271**, 108171 (2022).
[37] J. H. Los and A. Fasolino, Phys. Rev. B **68**, 024107 (2003).
[38] S. Tsuneyuki, M. Tsukada, H. Aoki, and Y. Matsui, Phys. Rev. Lett. **61**, 869 (1988).
[39] L. Woodcock, Chemical Physics Letters **10**, 257 (1971).
[40] J. Fayos, Journal of Solid State Chemistry **148**, 278 (1999).
[41] L. Levien, C. T. Prewitt, and D. J. Weidner, American Mineralogist **65**, 920 (1980).
[42] D. R. Peacor, Zeitschrift für Kristallographie - Crystalline Materials **138**, 274 (1973).
[43] A. Stukowski, Modelling and Simulation in Materials Science and Engineering **18**, 015012 (2009).